JCI insight

β_{IV}-Spectrin/STAT3 complex regulates fibroblast phenotype, fibrosis, and cardiac function

Nehal J. Patel, … , Keith J. Gooch, Thomas J. Hund

JCI Insight. 2019;4(20):e131046. https://doi.org/10.1172/jci.insight.131046.

Research Article **Cardiology** **Cell biology**

Increased fibrosis is a characteristic remodeling response to biomechanical and neurohumoral stress and a determinant of cardiac mechanical and electrical dysfunction in disease. Stress-induced activation of cardiac fibroblasts (CFs) is a critical step in the fibrotic response, although the precise sequence of events underlying activation of these critical cells in vivo remain unclear. Here, we tested the hypothesis that a β_{IV}-spectrin/STAT3 complex is essential for maintenance of a quiescent phenotype (basal nonactivated state) in CFs. We reported increased fibrosis, decreased cardiac function, and electrical impulse conduction defects in genetic and acquired mouse models of β_{IV}-spectrin deficiency. Loss of β_{IV}-spectrin function promoted STAT3 nuclear accumulation and transcriptional activity, and it altered gene expression and CF activation. Furthermore, we demonstrate that a quiescent phenotype may be restored in β_{IV}-spectrin–deficient fibroblasts by expressing a β_{IV}-spectrin fragment including the STAT3-binding domain or through pharmacological STAT3 inhibition. We found that in vivo STAT3 inhibition abrogates fibrosis and cardiac dysfunction in the setting of global β_{IV}-spectrin deficiency. Finally, we demonstrate that fibroblast-specific deletion of β_{IV}-spectrin is sufficient to induce fibrosis and decreased cardiac function. We propose that the β_{IV}-spectrin/STAT3 complex is a determinant of fibroblast phenotype and fibrosis, with implications for remodeling response in cardiovascular disease (CVD).

JCI insight

RESEARCH ARTICLE

β_{IV}-Spectrin/STAT3 complex regulates fibroblast phenotype, fibrosis, and cardiac function

Nehal J. Patel,[1,2] Drew M. Nassal,[1,2] Amara D. Greer-Short,[1,2] Sathya D. Unudurthi,[1,2] Benjamin W. Scandling,[1,2] Daniel Gratz,[1] Xianyao Xu,[1] Anuradha Kalyanasundaram,[1,3] Vadim V. Fedorov,[1,3] Federica Accornero,[1,3] Peter J. Mohler,[1,3,4] Keith J. Gooch,[1,2] and Thomas J. Hund[1,2,4]

[1]The Frick Center for Heart Failure and Arrhythmia, Dorothy M. Davis Heart and Lung Research Institute, The Ohio State University Wexner Medical Center, Columbus, Ohio, USA. [2]Department of Biomedical Engineering, College of Engineering, The Ohio State University, Columbus, Ohio, USA. [3]Department of Physiology and Cell Biology, and [4]Department of Internal Medicine, The Ohio State University Wexner Medical Center, Columbus, Ohio, USA.

Increased fibrosis is a characteristic remodeling response to biomechanical and neurohumoral stress and a determinant of cardiac mechanical and electrical dysfunction in disease. Stress-induced activation of cardiac fibroblasts (CFs) is a critical step in the fibrotic response, although the precise sequence of events underlying activation of these critical cells in vivo remain unclear. Here, we tested the hypothesis that a β_{IV}-spectrin/STAT3 complex is essential for maintenance of a quiescent phenotype (basal nonactivated state) in CFs. We reported increased fibrosis, decreased cardiac function, and electrical impulse conduction defects in genetic and acquired mouse models of β_{IV}-spectrin deficiency. Loss of β_{IV}-spectrin function promoted STAT3 nuclear accumulation and transcriptional activity, and it altered gene expression and CF activation. Furthermore, we demonstrate that a quiescent phenotype may be restored in β_{IV}-spectrin–deficient fibroblasts by expressing a β_{IV}-spectrin fragment including the STAT3-binding domain or through pharmacological STAT3 inhibition. We found that in vivo STAT3 inhibition abrogates fibrosis and cardiac dysfunction in the setting of global β_{IV}-spectrin deficiency. Finally, we demonstrate that fibroblast-specific deletion of β_{IV}-spectrin is sufficient to induce fibrosis and decreased cardiac function. We propose that the β_{IV}-spectrin/STAT3 complex is a determinant of fibroblast phenotype and fibrosis, with implications for remodeling response in cardiovascular disease (CVD).

Introduction

Cardiovascular disease (CVD) remains a leading cause of death worldwide (1). A common finding across multiple forms of CVD is increased cardiac fibrosis, leading to cardiac dysfunction and life-threatening arrhythmia (2–4). Cardiac fibroblasts (CFs) are collagen-producing cells distributed throughout the myocardium that form a fibrous structure to support organ function (2, 5). In response to injury, quiescent CFs undergo a remarkable activation process, characterized by phenotypic transition to a cell type with increased collagen production, proliferation, and contractility (e.g., myofibroblast) (4–6). Although a myriad of neurohumoral and biomechanical factors that promote CF activation have been identified, the precise mechanisms underlying phenotypic transition and activation of these critical cells in vivo remain unclear (4, 5, 7).

The spectrin-based cytoskeleton is an essential structure for the mechanical integrity of metazoan cell membranes (8, 9). The spectrin molecule forms as a flexible heterotetramer of α- and β-subunits with broad distribution of spectrin isoforms in mammalian tissues (2 α- and 5 β-spectrin isoforms expressed in humans) (9, 10). Mounting data support an expanded role for spectrins in not only providing mechanical support for membranes but also in coordination of critical cell signaling pathways (11). In particular, β_{IV}-spectrin has emerged as a dynamic scaffold that organizes local signaling domains for the regulation of ion channels and membrane excitability in multiple cell types (12–15). Recently, our group identified a role for β_{IV}-spectrin in control of gene transcription in the heart via association with signal transducer and activation of transcription 3 (STAT3) (16), a multifunctional transcriptional regulator involved in a variety of cellular responses including hypertrophy, proliferation, and survival (17–20).

Conflict of interest: The author have declared that no conflict of interest exists.

Submitted: June 13, 2019
Accepted: September 18, 2019
Published: October 17, 2019.

Reference information: *JCI Insight*. 2019;4(20):e131046. https://doi.org/10.1172/jci.insight.131046.

Importantly, loss of β_{IV}-spectrin in response to chronic pressure overload promotes dysregulation of STAT3-dependent gene expression, increased fibrosis, and cardiac dysfunction in mice (16).

Here, we used genetic and acquired mouse models of β_{IV}-spectrin deficiency, including an inducible fibroblast-specific β_{IV}-KO mouse, to test the hypothesis that the β_{IV}-spectrin/STAT3 complex is essential for maintenance of a quiescent phenotype in CFs. We propose that dysregulation of the spectrin-based complex promotes CF activation, fibrosis, and cardiac dysfunction. Our findings point to a previously unidentified pathway for controlling fibroblast phenotype and fibrosis in response to chronic stress in vivo.

Results

Increased fibrosis and cardiac dysfunction in the setting of β_{IV}-spectrin deficiency. Cardiac structure and function were first analyzed in 2 different models of β_{IV}-spectrin deficiency: (a) *qv^{4J}* mice that carry a spontaneous mutation in *Spnb4* resulting in expression of truncated β_{IV}-spectrin lacking STAT3 binding (16, 21); and (b) WT mice subjected to 6 weeks of transaortic constriction (TAC) to induce heart failure (acquired β_{IV}-spectrin deficiency) (16). Echocardiography revealed a significant decrease in ejection fraction in *qv^{4J}* animals compared with WT, although not to the level observed in WT TAC mice (Figure 1, A and B). In addition, *qv^{4J}* mice also showed decreased fractional shortening and left ventricular (LV) dilation, relative to WT baseline consistent with remodeling changes observed in WT TAC mice (Supplemental Table 1; supplemental material available online with this article; https://doi.org/10.1172/jci.insight.131046DS1). In addition to cardiac dysfunction, β_{IV}-spectrin–deficient animals displayed defects in cardiac electrical impulse propagation. Specifically, conduction velocity of electrical impulse propagation (evaluated in longitudinal and transverse directions) was reduced in both *qv^{4J}* and WT TAC hearts whereas inducibility of ventricular tachycardia (VT) was increased compared with WT baseline (Figure 1, C–F). Analysis of isolated myocytes revealed a highly eccentric growth in *qv^{4J}* myocytes with increased length-to-width ratio (aspect ratio) compared with WT (Supplemental Figure 1). Masson's trichrome staining of ventricular sections showed a marked increase in fibrosis in *qv^{4J}* hearts compared with WT, similar to the level observed in WT TAC hearts (Figure 2, TAC fibrosis levels similar to previous reports, ref. 16). Together these data define a wide array of cardiac remodeling changes, including mechanical and electrical dysfunction, linked to β_{IV}-spectrin deficiency.

β_{IV}-spectrin deficiency promotes nuclear accumulation of STAT3 in cardiac fibroblasts. The observation of increased fibrosis in β_{IV}-spectrin–deficient mice led us to ask whether CF function is directly affected by loss of β_{IV}-spectrin. Although our previous work has elucidated a role for β_{IV}-spectrin in regulating STAT3 signaling in myocytes (16), nothing is known about expression or function of the β_{IV}-spectrin/STAT3 complex in CFs. Therefore, expression of the complex was analyzed in isolated primary CFs from adult WT (baseline and TAC) and *qv^{4J}* hearts by immunostaining. Successful isolation of fibroblasts was verified by positive vimentin expression by immunoblotting and immunohistochemistry (Supplemental Figure 2). Prominent β_{IV}-spectrin immunoreactive signal was detectable in WT but not in *qv^{4J}* or WT TAC CFs (C-terminal antibody epitope and STAT3 binding motif absent in *qv^{4J}* allele, while total β_{IV}-spectrin expression is decreased in TAC; ref. 16) (Figure 3). Interestingly, STAT3 was found concentrated with β_{IV}-spectrin mostly along the membrane periphery in WT CFs (Figure 3A). In contrast, CFs from *qv^{4J}* and WT TAC hearts showed abnormal STAT3 cytoplasmic localization, with a substantial increase in STAT3 nuclear distribution compared with WT baseline (Figure 3, A and B). Immunoblotting showed no difference in the level of total STAT3 between the 3 groups (Supplemental Figure 2).

β_{IV}-spectrin deficiency alters cardiac fibroblast gene expression and activity. We next sought to determine whether loss of β_{IV}-spectrin affected CF phenotype (gene expression, activation state). STAT3 transcriptional activity was first assessed in WT and *qv^{4J}* CFs using a LUC reporter assay. Consistent with the increase in STAT3 nuclear localization, *qv^{4J}* CFs showed a marked increase in STAT3 transcriptional activity compared with WT (Figure 4A). In parallel, RNA sequencing and pathway analysis was performed on isolated WT and *qv^{4J}* CFs and revealed dramatic transcriptional changes induced by β_{IV}-spectrin deficiency with enrichment of genes involved in cell proliferation, motility, and differentiation (Supplemental Table 2). STAT3 was predicted to be a likely upstream mediator of observed transcriptional changes (P = 1.45e-12). Transcriptional changes in select genes were confirmed by quantitative PCR (qPCR) (Figure 4B). Additional genes previously identified as markers for an activated myofibroblast phenotype (22) were also assessed. Significant differences were observed between *qv^{4J}* and WT CFs in fibrotic genes *Col1a1* and *Vim* previously identified as regulated by STAT3 (16, 19, 23), but not other myofibroblast markers including *Acta2* (Supplemental Figure 3), suggesting a partial reprogramming

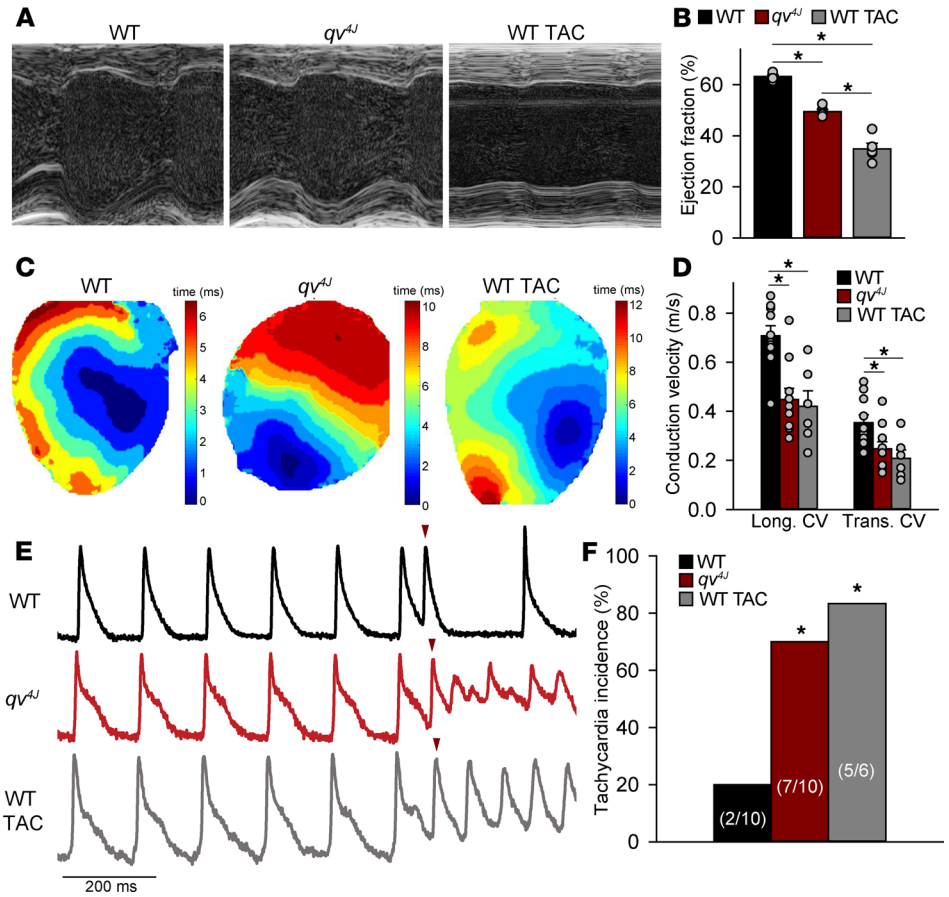

Figure 1. Cardiac mechanical and electrical dysfunction in the setting of β_{IV}-spectrin deficiency. (**A**) Representative echocardiograms from WT and *qv*^{4J} at baseline and from WT following 6 weeks of transaortic constriction (TAC) animals. (**B**) Summary data (mean ± SEM) for echocardiographic features. n = 5 animals for all groups; *P < 0.05 by 1-way ANOVA and Holm-Sidak post hoc pairwise comparison. (**C**) Representative activation maps of isolated, Langendorff perfused hearts during S1 pacing (cycle length = 150 ms). (**D**) Summary data (mean ± SEM) of conduction velocity in longitudinal (long) and transverse (trans) directions and provided in units of m/s. n = 10 hearts for WT and *qv*^{4J} and n = 6 for WT TAC; *P < 0.05 by 1-way ANOVA and Holm-Sidak post hoc pairwise comparison. (**E**) Optically recorded action potentials during programmed stimulation (S1S2 protocol) in isolated, Langendorff perfused hearts in WT baseline, *qv*^{4J} baseline, and WT TAC (Scale bar: 200 ms). Red arrow indicates initiation of S2 stimulus. Representative traces are shown for each heart at the longest S1S2 interval that resulted in tachycardia (demonstrated for *qv*^{4J} and WT TAC) or shortest S1S2 interval with successful capture (demonstrated for WT). (**F**) Summary data of ventricular tachycardia (VT) incidence following S1S2 pacing in WT baseline, *qv*^{4J} baseline, and WT TAC hearts. Inducibility was assessed over a range of S1S2 intervals, as described in Methods. n = 10 hearts for WT and *qv*^{4J} and n = 6 for WT TAC; *P < 0.05 by χ^2 test.

process perhaps analogous to an immature proto-myofibroblast state (7). Fibroblast proliferation was assessed to test for functional consequences of altered gene expression in the setting of β_{IV}-spectrin deficiency. A significant increase in proliferation (measured as BrdU intensity) was observed in *qv*^{4J} CFs at 6 and 12 hours following BrdU treatment compared with WT (Figure 4C). BrdU results were confirmed by manual counting of cells at the same time points (Supplemental Figure 2). Furthermore, *qv*^{4J} CFs showed a significant increase in contractility, assessed by collagen gel volume compaction rate, relative to WT (Figure 4, D and E). Together, these data demonstrate that loss of β_{IV}-spectrin alters CF gene expression and phenotype, producing a more active cell type. TGF-β levels are elevated in heart failure and have been linked to increased fibrosis (24). Therefore, the effect of TGF-β on β_{IV}-spectrin and related genes was assessed in isolated CFs. Interestingly, CFs treated with TGF-β showed a significant decrease in β_{IV}-spectrin together with changes in select genes differentially regulated in *qv*^{4J} CFs compared with WT (Supplemental Figure 4, compare to Figure 4B). As a first step in determining potential relevance of findings to humans, we performed acute β_{IV}-spectrin knockdown in human adult ventricular fibroblasts. An acute time course was used for optimal knockdown of β_{IV}-spectrin (72-hour transfection time per manufacturer's instructions) and confirmed by decreased β_{IV}-spectrin expression by qPCR and loss of

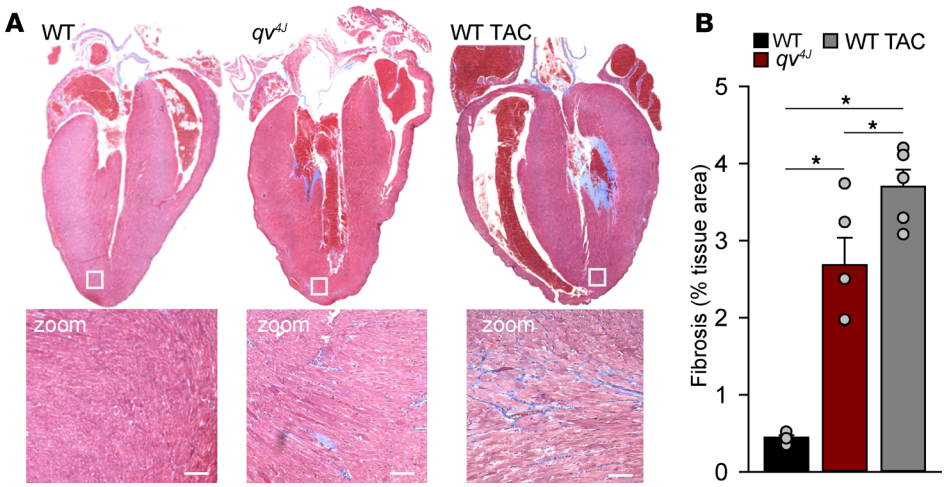

Figure 2. Increased fibrosis in mouse models of β_{IV}-spectrin deficiency. (**A**) Cardiac fibrosis was assessed by Masson's trichrome staining of ventricular heart sections (collagen labeled blue) from WT and *qv*^{4J} animals at baseline and from WT animals following 6 weeks of transaortic constriction (TAC). Original magnification, ×20 shown in zoom image with scale bars: 200 μm. (**B**) Summary data (mean ± SEM) showing fibrosis as percentage of tissue area. n = 5 where N is the number of hearts analyzed for each group (4 longitudinal sections of entire ventricles analyzed per heart). *$P < 0.05$ by 1-way ANOVA and Holm-Sidak post hoc pairwise comparison.

β_{IV}-spectrin immunoreactive signal in human CFs transfected with β_{IV}-spectrin siRNA (Supplemental Figure 5). Expression of select genes differentially expressed in *qv*^{4J} fibroblasts was assessed. A significant increase in *SERPINA3* was detected in β_{IV}-spectrin–deficient human CFs compared with control (scrambled siRNA) (Supplemental Figure 5), consistent with observations in the *qv*^{4J} mouse (other genes showed a nonsignificant trend).

Rescue of quiescent phenotype in qv^{4J} *fibroblasts*. To directly test the role of β_{IV}-spectrin in observed changes in *qv*^{4J} fibroblasts, *qv*^{4J} CFs were transfected with a β_{IV}-spectrin construct comprised of repeats 10 through the C-terminus ($\beta_{IV,10\text{-}C}$, containing putative STAT3 binding motif in repeat 15; ref. 16). Six days following transfection, *qv*^{4J} CFs expressing $\beta_{IV,10\text{-}C}$ showed extranuclear STAT3 distribution, in contrast with the mostly nuclear localization observed in *qv*^{4J} expressing empty vector and WT (Figure 5, A and B, and Supplemental Figure 6). Consistent with the redistribution of STAT3 out of the nucleus, *qv*^{4J} CFs expressing $\beta_{IV,10\text{-}C}$ displayed a decrease in proliferation as assessed by BrdU assay (Figure 5C). At the same time, *qv*^{4J} CFs treated with the STAT3 inhibitor S3I-201 showed a similar decrease in proliferation compared with vehicle control, supporting a role for STAT3 dysregulation in CF activation in the setting of β_{IV}-spectrin deficiency (Figure 5D).

STAT3 inhibition abrogates cardiac fibrosis and dysfunction in the setting of β_{IV}-spectrin deficiency. To determine whether rescue of the β_{IV}-spectrin–deficient CF phenotype with STAT3 inhibition translated to functional improvement in vivo, we treated *qv*^{4J} and WT animals with S3I-201 (20 mg/kg i.p. injection daily) or vehicle (3% DMSO in PBS) for 2 weeks. Echocardiography revealed significant improvement in ejection fraction in *qv*^{4J} treated with S3I-201 compared with WT (Figure 6, A and B). In addition, Masson's trichrome staining revealed a significant decrease in fibrosis in *qv*^{4J} mice treated with S3I-201 compared with vehicle (Figure 6, C and D).

Fibroblast-specific KO of β_{IV}-spectrin induces fibrosis and cardiac dysfunction. To determine the specific contribution of fibroblasts to cardiac dysfunction observed in our in vivo models of global β_{IV}-spectrin deficiency, we generated a tamoxifen-inducible fibroblast-specific β_{IV}-spectrin–KO mouse (β_{IV}ifKO) by cross breeding periostin^{MerCreMer} with β_{IV}-spectrin–floxed mice (β_{IV}ifKO, Figure 7A). It has been shown that periostin is specifically expressed in activated CFs (22) and that treatment with angiotensin II increases periostin expression in the heart (ref. 25 and Supplemental Figure 7). Therefore, β_{IV}-ifKO and control (β_{IV}-floxed, Cre-) mice were treated for 2 weeks with tamoxifen/angiotensin II to ensure robust activation of the periostin promoter, MerCreMer, and subsequent β_{IV}-spectrin–KO in CFs. β_{IV}-ifKO fibroblasts showed similar transcriptional changes to those observed in *qv*^{4J} (compare Figure 7B and Figure 4B) together with a loss of β_{IV}-spectrin and STAT3 mislocalization, without altering myocyte β_{IV}-spectrin expression (Figure 7, C–E and Supplemental Figure 8). In parallel, β_{IV}-ifKO mice showed increased fibrosis (Figure 7, F and G) and decreased cardiac function (Figure 7, H and I and Supplemental Table 3) compared with control mice, supporting a role for fibroblast reprogramming in cardiac dysfunction in the setting of β_{IV}-spectrin deficiency.

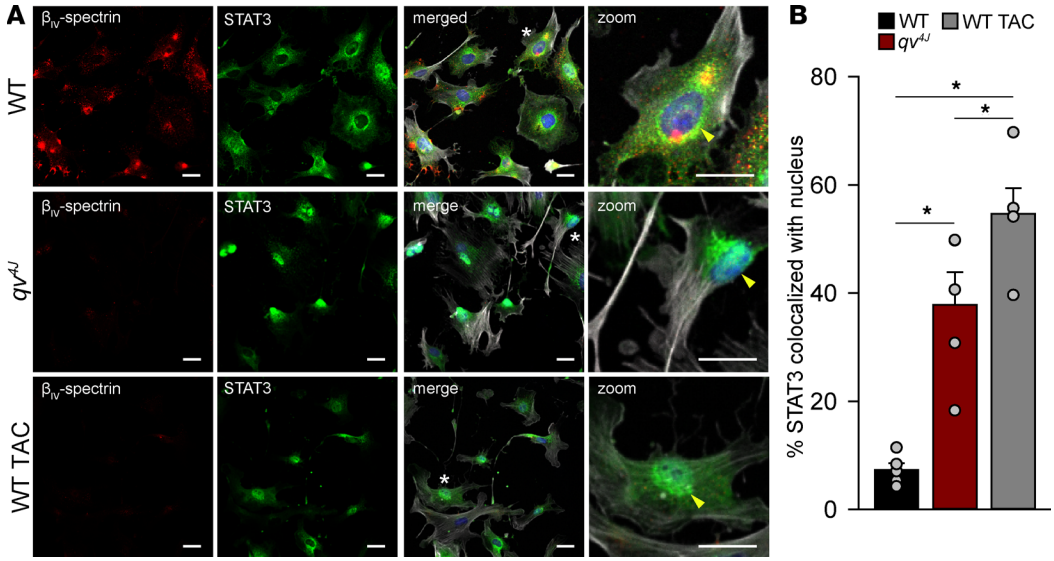

Figure 3. β_{IV}-spectrin deficiency promotes STAT3 relocalization in cardiac fibroblasts. (**A**) Representative confocal microscopy images (original magnification, ×10) of permeabilized adult WT, *qv*^{4J}, and WT TAC cardiac fibroblasts (CFs) immunostained for β_{IV}-spectrin (red), STAT3 (green; yellow arrow indicates nucleus border), phalloidin (gray in merged image), and DAPI (blue in merged image). White asterisk in merged images indicates region of zoom shown in far right panel. Yellow arrow in zoom image indicates nucleus border. Scale bar: 20 μm. (**B**) Summary data (mean ± SEM) of STAT3 nuclear localization in WT, *qv*^{4J}, and WT TAC CFs. n = 5 per group where N is the number of hearts (5 cells analyzed per heart); *$P < 0.05$ by 1-way ANOVA and Holm-Sidak post hoc pairwise comparison.

Discussion

Here we define a role for β_{IV}-spectrin in tuning the phenotype of CFs via changes in STAT3 subcellular distribution. Mechanistically, we demonstrated that loss of β_{IV}-spectrin, as observed in TAC, promotes nuclear accumulation of STAT3 and CF activation resulting in a more proliferative, contractile cell type. Ultimately, these changes at the cellular level result in increased fibrosis, cardiac remodeling, and defects in electrical impulse propagation. Based on our findings, we anticipate that the β_{IV}-spectrin/STAT3 complex will prove an effective target for improving both cardiac mechanical and electrical function in the setting of complex disease (e.g., heart failure).

STAT3 has emerged as an important multifunctional transcriptional regulator of fibrosis, proliferation, ECM synthesis, survival, and growth (17). Previous studies have demonstrated that STAT3 is dysregulated in systemic sclerosis and serves as a crucial checkpoint for fibroblast activation and tissue fibrosis in the skin (19). In CFs, it has been shown that miR-21 induces STAT3 activation resulting in increased proliferation with upregulation of α-smooth muscle actin, collagen I, and collagen III promoting atrial fibrillation in mice, whereas S31-201 promoted downregulation of miR-21 abrogating myofibroblast activation, fibrosis, and atrial arrhythmogenesis (18). At the same time, other studies have shown that constitutive STAT3 activation via IL-6 promotes and enhances CF collagen biosynthesis and activation in vitro, whereas STAT3 suppression abrogates deposition of extracellular matrix in mice following myocardial infarction (26). Similarly, IL-6 deletion has been shown to prevent STAT3 phosphorylation, abrogate fibrosis, and improve cardiac function following TAC (27). STAT3 activation has also been identified downstream of excess TGF-β, leading to increased CF extracellular matrix production (20). Our findings add to the growing literature supporting STAT3 as a critical regulator of cardiac fibrosis. Importantly, our results demonstrate that fibroblast-specific dysregulation of the STAT3 signaling is sufficient to induce cardiac fibrosis. Moreover, our data identify an alternative pathway for noncanonical activation of STAT3 downstream of β_{IV}-spectrin dysfunction.

Although we demonstrated that STAT3 inhibition abrogates CF phenotype changes and remodeling observed in β_{IV}-spectrin–deficient mice, we cannot rule out involvement of other signaling pathways. In this manner, it is interesting to consider how the β_{IV}-spectrin/STAT3 axis explored here interacts with other signaling pathways known to be involved in fibroblast activation and fibrosis. For example, the TGF-β/SMAD signaling pathway is well established as an important node for regulating fibroblast gene expression and phenotype (5, 28, 29). Interestingly, mice deficient in embryonic liver fodrin (ELF, also

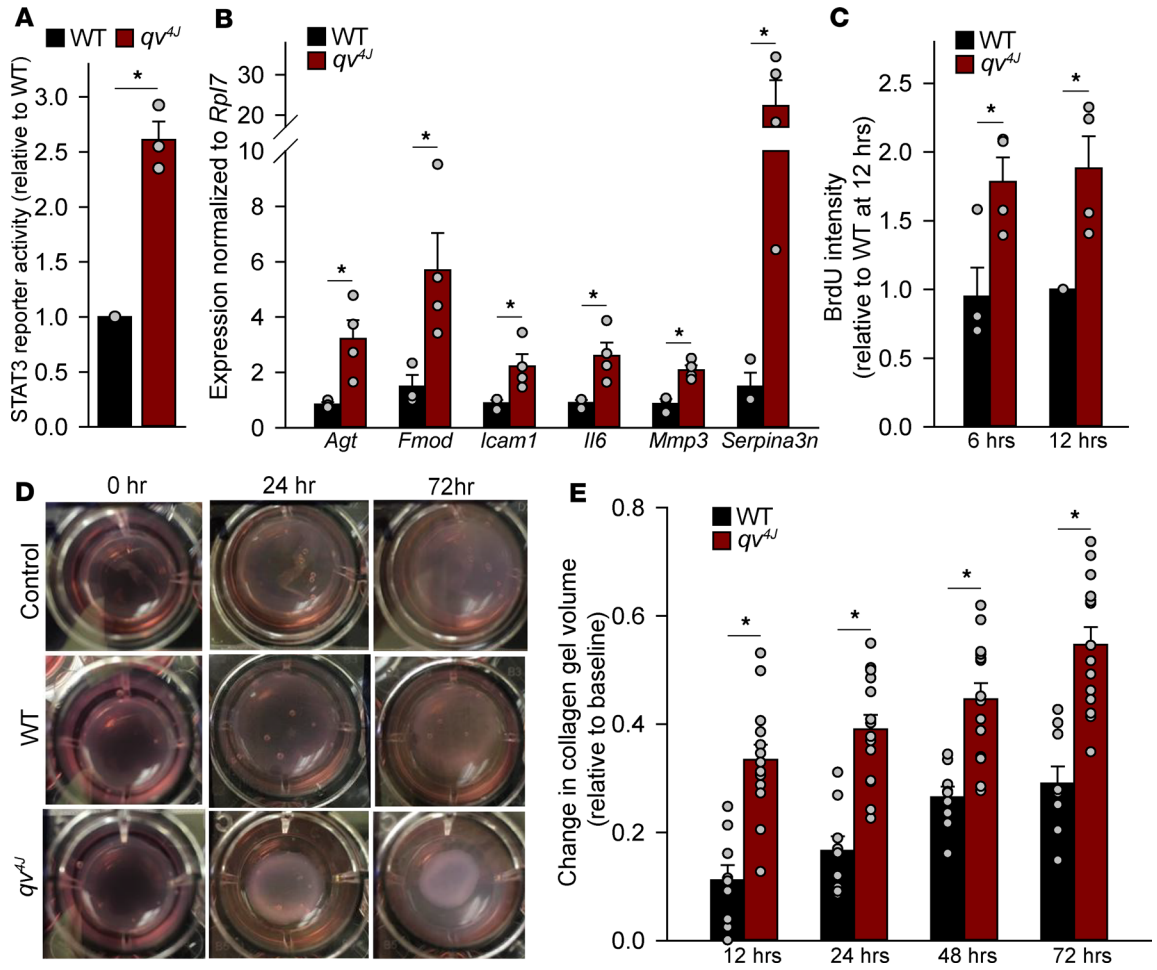

Figure 4. β_{IV}-spectrin deficiency alters STAT3 transcriptional activity, gene expression, and activity of cardiac fibroblasts. (**A**) Summary data (mean ± SEM) of STAT3 transcriptional activity in WT and *qv*^{4J} cardiac fibroblasts (CFs) transfected with STAT3 luciferase reporter. n = 3 per group where N is the number of independent preparations for each genotype; *P < 0.05 by 2-tailed t test. (**B**) Expression of select genes (relative to *Rpl7*) determined by qPCR in WT and *qv*^{4J} CFs. Data presented as mean ± SEM; n = 3 for WT and n = 4 for *qv*^{4J} where N is the number of independent preparations; *P < 0.05 by 2-tailed t test. (**C**) Summary data (mean ± SEM) of BrdU intensity measured at 6 and 12 hours following BrdU treatment in WT and *qv*^{4J} CFs as a measure of proliferation (levels normalized to WT at 12 hours). n = 4 independent preparations for each genotype; *P < 0.05 by 2-tailed t test. (**D**) Representative images of collagen gels seeded with WT or *qv*^{4J} CFs over 72-hour time course. Collagen gels without seeded cells (control) are shown for comparison. (**E**) Summary data (mean ± SEM) of change in collagen gel volume over the 72-hour time course in WT and *qv*^{4J} CFs. n = 9 for WT and n = 14 for *qv*^{4J}, where N represents the number of independent preparations; *P < 0.05 by 2-tailed t test.

referred to as β_{II}-spectrin) show mislocalization of SMAD3/4 and loss of TGF-β–dependent transcriptional response in mouse embryonic fibroblasts (30). More recently, TGF-β has been shown to induce degradation of α_{II}- and β_{II}-spectrin subunits in dermal fibroblasts (31), although the authors did not identify an involvement in downstream effects (β_{IV}-spectrin isoform was not studied). Our findings show that TGF-β promotes loss of β_{IV}-spectrin in CFs (Supplemental Figure 4). Based on this previous work and our findings, it will be interesting to determine whether there is a functional link between TGF-β/SMAD and β_{IV}-spectrin/STAT3 pathways in controlling CF phenotype or whether they represent parallel networks that respond to distinct stress stimuli. Furthermore, these data, together with our previous observation that CaMKII activation induces downregulation of β_{IV}-spectrin (16), suggest that β_{IV}-spectrin integrates several upstream pathological signals to induce cardiac remodeling.

Recent lineage tracing studies have shown that myocardial infarction induces activation of quiescent, resident CFs in the infarct border region, which then infiltrate the central infarct zone to facilitate scar generation and maintenance (6). Although our studies focused on reactive fibrosis in the setting of chronic pressure overload, we anticipate that a similar dysfunction occurs in the infarct border zone where Ca^{2+}/calmodulin kinase II is activated to potentially promote β_{IV}-spectrin degradation (16, 32, 33). Based on

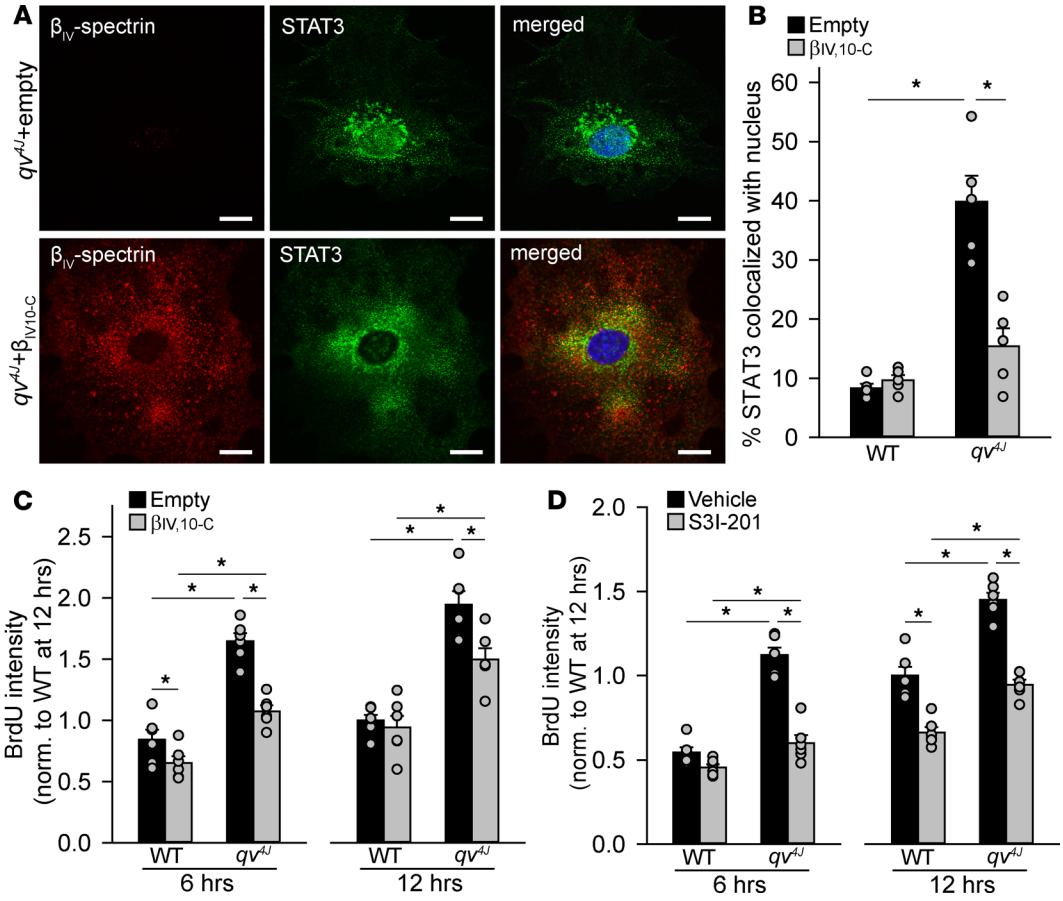

Figure 5. Rescue of quiescent fibroblast phenotype in β_{IV}-spectrin–deficient fibroblasts. (**A**) Representative confocal microscopy images (original magnification, ×40) of permeabilized adult *qv*^{4J} cardiac fibroblasts (CFs) immunostained for β_{IV}-spectrin (red), STAT3 (green), and DAPI (blue in merged image) following transfection of empty vector plasmid (control) or $\beta_{IV,10\text{-}C}$ rescue construct (scale bar: 5 μm). (**B**) Summary data (mean ± SEM) of STAT3 nuclear localization in WT and *qv*^{4J} CFs transfected with empty vector or $\beta_{IV,10\text{-}C}$. *$P < 0.05$ by 1-way ANOVA with Holm-Sidak post hoc pairwise comparison; $n = 5$ per group where N is the number of independent preparations (5 cells analyzed per preparation). (**C** and **D**) Summary data (mean ± SEM) of BrdU intensity measured at 6 and 12 hours following BrdU treatment in WT and *qv*^{4J} CFs either (**C**) transfected with empty vector or $\beta_{IV,10\text{-}C}$, or (**D**) treated with STAT3 inhibitor S3I-201 (100 μM) or vehicle (3% DMSO in PBS). $n = 6$ independent preparations for each group; data normalized to WT control (empty vector or vehicle) at 12 hours; *$P < 0.05$ by 1-way ANOVA with Holm-Sidak post hoc pairwise comparison.

these findings, it is interesting to consider the possibility that loss of β_{IV}-spectrin is a critical step in CF activation important for myocardial repair following myocardial infarction.

Although this work focuses on the contribution of fibroblasts to dysfunction induced by spectrin deficiency, we have found in our previous work that cardiomyocyte-specific deletion of β_{IV}-spectrin results in fibrosis (16). It will be interesting to determine how myocytes, fibroblasts, and other cells communicate in vivo to coordinate the organ level response to stress. Going forward, it will be equally important to determine how our findings in the mouse translate to human disease. Recently, several loss-of-function variants in β_{IV}-spectrin have been identified in human patients with neuropathy, myopathy, and congenital deafness (34, 35). We anticipate that our findings will have important implications for human patients with both acquired and inherited forms of disease, given: (a) conservation of the β_{IV}-spectrin/STAT3 complex across mouse and humans; (b) our previous studies showing loss of β_{IV}-spectrin in human heart failure (36); and (c) results from this study showing transcriptional changes in human fibroblasts with acute spectrin knockdown (Supplemental Figure 5).

In this study, we sought to determine whether fibroblasts have a role in cardiac remodeling induced by β_{IV}-spectrin deficiency using a β_{IV}-ifKO mouse model. Although these studies indicate that fibroblasts contribute directly to dysfunction, it is important to note that the model uses angiotensin II to increase expression of periostin, thereby driving fibroblast-specific β_{IV}-spectrin deletion. Angiotensin II has been shown to induce fibroblast activation and fibrosis (37). However, this confounding variable is mitigated by the observation that angiotensin II-treated β_{IV}-ifKO mice show a greater extent of fibrosis

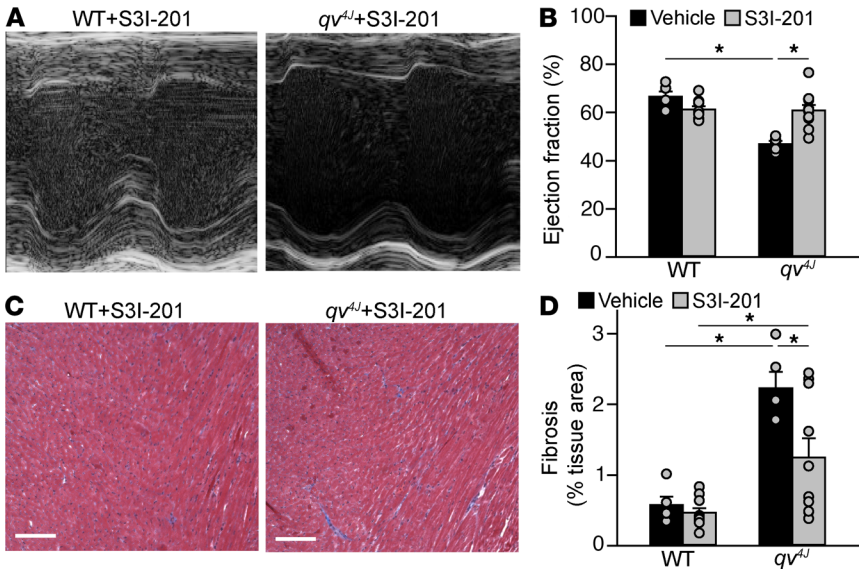

Figure 6. STAT3 inhibition normalizes fibrosis and cardiac function in β_{IV}-spectrin–deficient mice. (**A**) Representative echocardiograms from WT and *qv*^{4J} animals following 2 weeks of treatment with the STAT3 inhibitor S3I-201 (20 mg/kg i.p. injection daily) or vehicle (3% DMSO in PBS). (**B**) Summary data (mean ± SEM) of the percent change in ejection fraction in WT and *qv*^{4J} animals following 2 weeks of S3I-201 or vehicle treatment. n = 10 animals for each group; *P < 0.05 by 1-way ANOVA with Holm-Sidak post hoc pairwise comparison. (**C**) Representative Masson's trichrome–stained ventricular sections (collagen labeled blue, original magnification, ×20) from WT and *qv*^{4J} animals after 2 weeks of S3I-201 or vehicle treatment. Scale bar: 200 μm. (**D**) Summary data (mean ± SEM) of the percent change in fibrosis in WT and *qv*^{4J} animals following 2 weeks of S3I-201 or vehicle treatment. n = 10 for both genotypes with S31-201; n = 5 for both genotypes with vehicle where N is the number of hearts (4 longitudinal sections of entire ventricles analyzed per heart); *P < 0.05 by 1-way ANOVA with Holm-Sidak post hoc pairwise comparison.

and cardiac dysfunction compared with angiotensin II-treated WT mice. Finally, although our studies focus on fibrosis as a driving factor for cardiac dysfunction, it is likely that coordinated changes in other factors (e.g., hypertrophy, angiogenesis) contribute to the overall phenotype in the setting of β_{IV}-spectrin deficiency. Notably, *qv*^{4J} myocytes show a highly eccentric myocyte growth (Supplemental Figure 1) that would be expected to drive LV dilation and impaired systolic function. It will be exciting for future studies to carefully dissect the interplay of these different tissue-level remodeling changes.

Methods

Mouse models. Adult (2–4 months) C57BL/6J male and female wildtype (WT, control) and truncated β_{IV}-spectrin (*qv*^{4J}) littermate mice were used. The *qv*^{4J} mice were obtained from Jackson Laboratory and express a *Sptnb4* allele with a spontaneous insertion point mutation at C4234T (Q1358→Stop) resulting in a premature stop codon proximal to the STAT3 binding region in β_{IV}-spectrin (21, 36). periostin^{MerCreMer} mice (22) were cross-bred with β_{IV}-spectrin floxed mice (16) to obtain tamoxifen-inducible β_{IV}-ifKO mice. Adult male and female β_{IV}-ifKO or control (β_{IV}-spectrin floxed, Cre-) mice were fed a diet containing 400 mg/kg tamoxifen citrate (Envigo) and treated with tamoxifen (MilliporeSigma) dissolved in corn oil (75 mg/kg i.p. injection daily) and angiotensin II (2.16 mg/kg i.p. injection daily) for 2 weeks to ensure robust activity of MerCreCre under Postn promoter (6, 38).

Optical mapping of ex vivo heart preparations. Optical mapping techniques were used to measure the electrical impulse propagation in the anterior portion of the isolated heart, as described (39). Briefly, hearts were perfused with oxygenated Tyrode's solution (at 37°C and pH of 7.4) via the aorta using a rolling pump at 2 mL/min. Tyrode's solution was comprised of 140 mM NaCl, 1.0 mM $MgCl_2$*$6H_2O$, 1.2 mM NaH_2PO_4, 4.0 mM KCl, 1.8 mM $CaCl_2$*$2H_2O$, 5.6 mM glucose, and 10 mM HEPES sodium salt. The motion uncoupler, Blebbistatin (from stock solution of 5 mg/mL in DMSO), was perfused for 15 minutes to obtain clear signal production with minimal alteration to electrophysiology. The voltage-sensitive dye, di-4-ANEPPS (4 μM) was subsequently perfused for 15 minutes. Images were obtained to verify that the dye successfully reached the extremities of the tissue. The LEX2-LZ4-G light source (SciMedia) with a 531/40 filter was used to

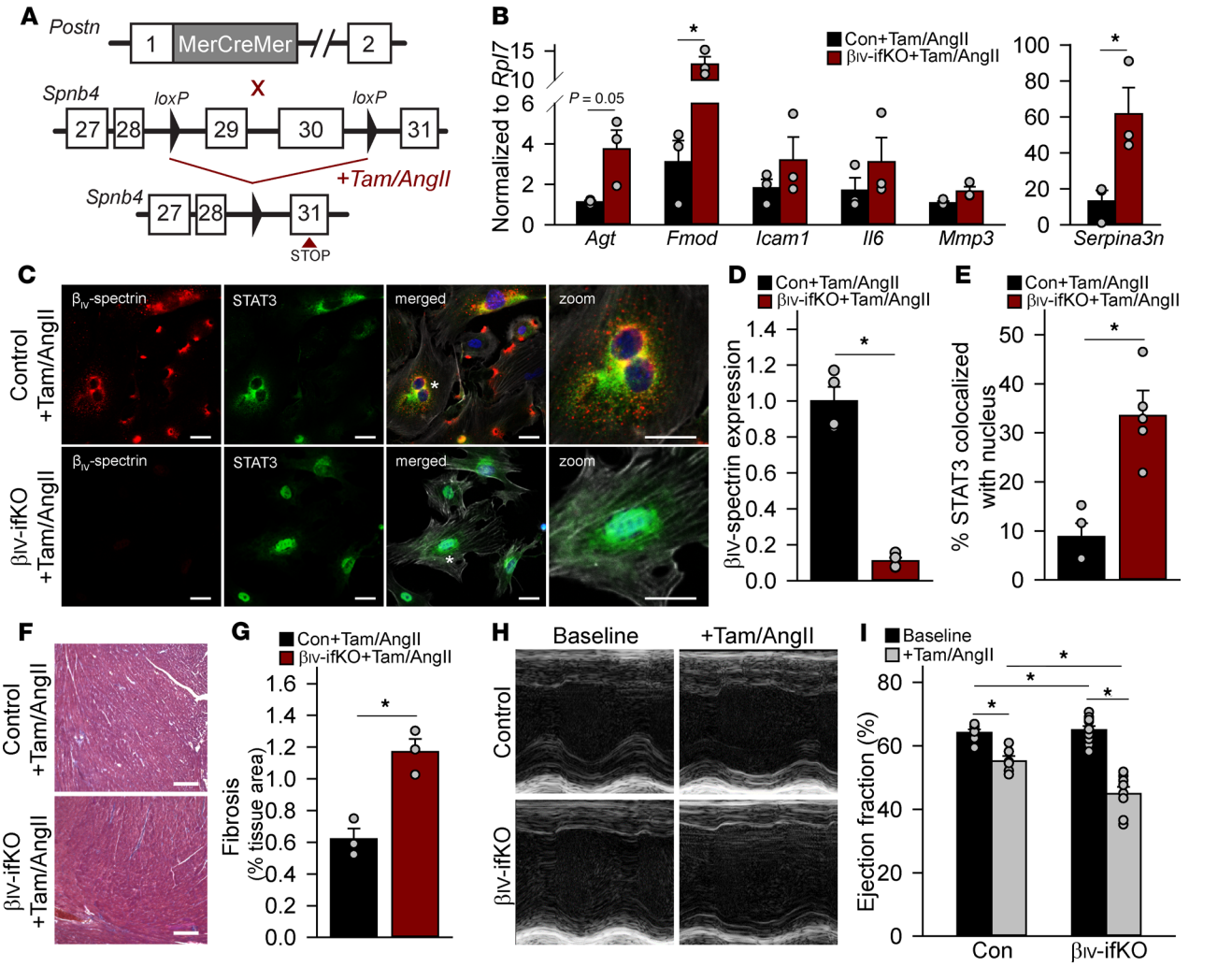

Figure 7. Fibroblast-specific deletion of β_{IV}-spectrin leads to altered gene expression and STAT3 dysregulation in cardiac fibroblasts (CFs) together with decreased cardiac function and fibrosis. (**A**) The β_{IV}-spectrin floxed mouse was cross-bred with the periostin^{MerCreMer} mouse to generate an inducible fibroblast-specific β_{IV}-spectrin KO mouse (β_{IV}-ifKO). Two-week treatment of animals with angiotensin II (2.16 mg/kg i.p. injection daily) together with tamoxifen (75 mg/kg i.p. injection daily) (+Tam/Ang II) was used to ensure robust activity of periostin^{MerCreMer} (periostin highly expressed in activated fibroblasts) and effective β_{IV}-spectrin KO in cardiac fibroblasts (22). (**B**) Expression of select fibrotic genes (relative to *Rpl7*) determined by qPCR in CFs isolated from control (β_{IV}-spectrin floxed, Cre-) and β_{IV}-ifKO following 2 weeks of tamoxifen/angiotensin II treatment (+tam/AngII). Data presented as mean ± SEM; n = 3 for control and n = 4 for β_{IV}-ifKO where N is the number of independent preparations; *P < 0.05 by 2-tailed t test. (**C**) Representative confocal microscopy images (original magnification, ×10) of permeabilized adult control and β_{IV}-ifKO CFs immunostained for β_{IV}-spectrin (red), STAT3 (green), phalloidin (gray in merged image), and DAPI (blue in merged image). White asterisk in merged images indicates region of zoom shown in far right panel. Scale bar: 20 mm. (**D** and **E**) Summary data (mean ± SEM) of β_{IV}-spectrin immunoreactive signal (normalized to DAPI) and STAT3 nuclear localization in control and β_{IV}-ifKO CFs. n = 4 per group where N is the number of independent preparations (5 fields analyzed per preparation for β_{IV}-spectrin and 5 cells analyzed per preparation for STAT3 nuclear localization); *P < 0.05 by 2-tailed t test. (**F**) Masson's trichrome–stained ventricular heart sections (collagen labeled blue, original magnification, ×20). Scale bars: 200 μm. (**G**) Summary data (mean ± SEM) showing fibrosis as percentage of tissue area. n = 3 different hearts for each group (4 longitudinal sections of entire ventricles analyzed per animal); *P < 0.05 by 1-way ANOVA and Holm-Sidak post hoc pairwise comparison. (**H**) Representative echocardiograms and (**I**) summary data (mean ± SEM) for ejection fraction from control and β_{IV}-ifKO animals at baseline and following 2 weeks of tamoxifen/angiotensin II treatment. n = 7 for control baseline; n = 6 for control+tam/AngII; n = 10 for β_{IV}-ifKO baseline; n = 8 for β_{IV}-ifKO+tam/AngII where N represents the number of animals; *P < 0.05 by 1-way ANOVA and Holm-Sidak post hoc pairwise comparison.

excite the dye. The MiCAM05 camera with a 600-mn long-pass filter was used to capture optical signals at 1000 Hz (1 ms/frame). Resulting images had an area of 1.06 × 1.06 cm^2. Custom-designed Zang Analysis MATLAB program was executed to obtain values from optical signals measured during programmed stimulation (40). AP duration at 80% repolarization (APD_{80}) was measured from optical signals throughout the mapped heart. Conduction velocity was measured and analyzed in transverse and longitudinal directions. Activation maps of stimulus 1 pacing were generated in RHYTHM software via MATLAB program (41).

The following S1S2 protocol was used to assess inducibility of VT: 6 s of S1 pacing at a cycle length of 150 ms was followed by a S2 stimulus at a S1S2 interval which decreased from 100 ms in increments of 10 ms until VT (defined as 3 or more successive beats) was observed or 1:1 capture failed.

Isolation of primary mouse and human ventricular cardiac fibroblasts. Mouse CFs were isolated from left and right ventricles under sterile conditions, as described (42). Human CFs were enzymatically isolated from nonfailing, LV tissue, as described (43). Briefly, mouse or human tissue was minced in 2 mg/mL collagenase II (Worthington) dissolved in 1× Ham's F-10 buffer (Corning). After digestion, the extract was filtered and centrifuged. The supernatant was discarded and cells were resuspended in DMEM; 1×, supplemented with 10% FBS, 1% L-glutamine, and 1% Pen/Strep. Cells were allowed to adhere to culture plates for approximately 4 to 5 hours prior to media removal containing nonadherent cells (e.g., endothelial, myocytes). Fresh feeding media was replenished, and cells were grown for 5 to 7 days to 80% to 100% confluency at 37°C in 5% CO_2. A subset of WT CFs was stimulated with TGF-β1 (10 ng/mL, R&D Systems) or vehicle control (1× PBS) for 48 hours, following 24 hours of serum starvation. All cell experiments were conducted at passage one (P1) unless otherwise noted.

Transfection of primary mouse and human cardiac fibroblasts. Isolated mouse CFs were transfected with $\beta_{IV,10\text{-}C}$ plasmid (1500 mg) or empty vector (1500 mg, control). Plasmids were generated as previously described (16). For transfection, lipofectamine 2000 (Invitrogen) was mixed with $\beta_{IV,10\text{-}C}$ plasmid and added to CFs for a 4-hour transfection incubation with serum starvation. CFs were then cultured for 6 days with normal feeding media. In parallel experiments, WT and qv^{4J} CFs were treated for 48 hours with S3I-201 (100 μM) or vehicle control (3% DMSO in 1× PBS) for 48 hours. Acute knockdown of β_{IV}-spectrin was achieved in human CFs by transfecting cells for 4 hours under serum starvation with lipofectamine RNAiMAX (Invitrogen) mixed with human siRNA SASI_Hs02_00354399 (10 μM) and SASI_Hs02_00357989 (10 μM), or SIC001-MISSION siRNA universal negative control (10 μM) (Sigma-Aldrich). CFs were then cultured for 72 hours with normal feeding media.

Proliferation assay. CFs were seeded into 96-well culture-treated plates, as described (44). Briefly, cells were adhered for 24 hours with serum starvation. Proliferation was then assessed for 12 hours through incorporation of BrdU, 5x. BrdU proliferation assay (Cell Signaling) was used to quantify proliferation rates (via colorimetric assessment) at desired time points of 6 and 12 hours based on manufacturer's protocol. Results were validated in a subset of experiments by manual cell counting using a hemocytometer. Experiments were conducted in technical triplicates.

Collagen gel formation and macroscopic gel contraction measurements. Type I rat-collagen gels (2 mg/mL) were prepared by mixing 10x PBS, sterile H_2O, acidic rat tail collagen, and 1M NaOH. Cells were added (500,000 cells/mL) and mixed before gelation. Cell-collagen mixtures were cast into 24-well culture plates and incubated at 37°C in 5% CO_2 for 1 hour. After incubation, 1 mL of culture feeding media was added, and the gels were released from wells to subject for floating. Collagen gels were photographed at various time points for 72 hours. Photographs were obtained prior to the start of the experiment and at regular intervals thereafter. Photographs were analyzed using NIH ImageJ software. Specifically, the diameter of each gel was measured in perpendicular directions and then averaged. As previously described, isotropic compaction was assumed to measure the volume ratio of gels before and after compaction (45). Gels without cells served as controls. Experiments were conducted in technical triplicates.

STAT3 reporter assay. STAT3 transcriptional activity in CFs was evaluated via a STAT3 plasmid (pGL4.47, Promega, 10 μg). Specifically, lipofectamine (Invitrogen) was mixed with the plasmid and added to CFs for a 4-hour transfection incubation with serum starvation. CFs were then cultured for 48 hours with normal feeding media. After 48 hours of culture, cells were lysed, and LUC activity was measured using Promega Dual LUC Reporter Assay according to manufacturer's protocol. Experiments were conducted in technical triplicates in 96-well plate. Relative LUC activity was quantitatively measured as the ratio of firefly (reporter) to Renilla (normalization, control) activity.

Statistics. SigmaPlot 14.0 was used for statistical analysis. A 2-tailed *t* test was used to determine *P* values for single comparisons. For multiple comparisons, a 1-way ANOVA with Holm-Sidak post hoc test was used (data presented as mean ± SEM). The null hypothesis was rejected for *P* value < 0.05.

Study approval. Animal studies were conducted in accordance with the *Guide for the Care and Use of Laboratory Animals* published by the National Institutes of Health (NIH) following protocols that were reviewed and approved by the IACUC at The Ohio State University. Nonfailing hearts were obtained through the Lifeline of Ohio Project. The local institutional review board approved the use of human subject tissue. This investigation conforms to the principles outlined in the Declaration of Helsinki.

See Supplemental Material for additional methods and primer sequences for qPCR (Supplemental Tables 4 and 5).

Author contributions

NJP, DMN, ADGS, SDU, BWS, and TJH designed the research studies. NJP, DMN, ADGS, SDU, BWS, XX conducted the experiments. NJP, DMN, ADGS, SDU, BWS, DG, and TJH analyzed the data. AK, VVF, FA, PJM, and KJG provided regents, samples, equipment, or animals. NJP and TJH wrote the manuscript. NJP, KJG, PJM, and TJH edited the manuscript.

Acknowledgments

The authors are supported by NIH (grant numbers HL114893, HL135096 to TJH, HL134824 to TJH and PJM, HL114383 and HL135754 to PJM; HL121284 and HL136951 to FA; HL115580 and HL135109 to VVF; NJP has support from T32 HL134616); James S. McDonnell Foundation and Saving Tiny Hearts Society (to TJH); American Heart Association (Postdoctoral fellowships to SDU, ADGS, and DMN); a TriFit Challenge grant from Ross Heart Hospital and Davis Heart and Lung Research Institute; and the OSU Comprehensive Cancer Center Genomics Shared Resource (P30CA016058). The authors thank the Lifeline of Ohio Organ Procurement Organization for providing the explanted hearts. The human heart repository program is supported by the Davis Heart and Lung Research Institute.

Address correspondence to: Thomas J. Hund, The Dorothy M. Davis Heart and Lung Research Institute, The Ohio State University Wexner Medical Center, 473 W. 12th Avenue, Columbus, Ohio 43210, USA. Phone: 614.292.0755; Email: Thomas.Hund@osumc.edu.

1. Benjamin EJ, et al. Heart Disease and Stroke Statistics-2017 Update: A Report From the American Heart Association. *Circulation*. 2017;135(10):e146–e603.
2. Travers JG, Kamal FA, Robbins J, Yutzey KE, Blaxall BC. Cardiac fibrosis: the fibroblast awakens. *Circ Res*. 2016;118(6):1021–1040.
3. Gourdie RG, Dimmeler S, Kohl P. Novel therapeutic strategies targeting fibroblasts and fibrosis in heart disease. *Nat Rev Drug Discov*. 2016;15(9):620–638.
4. Kong P, Christia P, Frangogiannis NG. The pathogenesis of cardiac fibrosis. *Cell Mol Life Sci*. 2014;71(4):549–574.
5. Tallquist MD, Molkentin JD. Redefining the identity of cardiac fibroblasts. *Nat Rev Cardiol*. 2017;14(8):484–491.
6. Fu X, et al. Specialized fibroblast differentiated states underlie scar formation in the infarcted mouse heart. *J Clin Invest*. 2018;128(5):2127–2143.
7. Stempien-Otero A, Kim DH, Davis J. Molecular networks underlying myofibroblast fate and fibrosis. *J Mol Cell Cardiol*. 2016;97:153–161.
8. Baines AJ, Pinder JC. The spectrin-associated cytoskeleton in mammalian heart. *Front Biosci*. 2005;10:3020–3033.
9. Bennett V, Baines AJ. Spectrin and ankyrin-based pathways: metazoan inventions for integrating cells into tissues. *Physiol Rev*. 2001;81(3):1353–1392.
10. Bennett V, Lorenzo DN. Spectrin- and ankyrin-based membrane domains and the evolution of vertebrates. *Curr Top Membr*. 2013;72:1–37.
11. Unudurthi SD, Greer-Short A, Patel N, Nassal D, Hund TJ. Spectrin-based pathways underlying electrical and mechanical dysfunction in cardiac disease. *Expert Rev Cardiovasc Ther*. 2018;16(1):59–65.
12. Berghs S, et al. βIV spectrin, a new spectrin localized at axon initial segments and nodes of ranvier in the central and peripheral nervous system. *J Cell Biol*. 2000;151(5):985–1002.
13. Komada M, Soriano P. βIV-spectrin regulates sodium channel clustering through ankyrin-G at axon initial segments and nodes of Ranvier. *J Cell Biol*. 2002;156(2):337–348.
14. Hund TJ, et al. A β(IV)-spectrin/CaMKII signaling complex is essential for membrane excitability in mice. *J Clin Invest*. 2010;120(10):3508–3519.
15. Kline CF, et al. βIV-Spectrin and CaMKII facilitate Kir6.2 regulation in pancreatic beta cells. *Proc Natl Acad Sci U S A*. 2013;110(43):17576–17581.
16. Unudurthi SD, et al. βIV-Spectrin regulates STAT3 targeting to tune cardiac response to pressure overload. *J Clin Invest*. 2018;128(12):5561–5572.
17. Haghikia A, Ricke-Hoch M, Stapel B, Gorst I, Hilfiker-Kleiner D. STAT3, a key regulator of cell-to-cell communication in the heart. *Cardiovasc Res*. 2014;102(2):281–289.
18. Huang Z, et al. Signal transducer and activator of transcription 3/MicroRNA-21 feedback loop contributes to atrial fibrillation by promoting atrial fibrosis in a rat sterile pericarditis model. *Circ Arrhythm Electrophysiol*. 2016;9(7):e003396.
19. Chakraborty D, et al. Activation of STAT3 integrates common profibrotic pathways to promote fibroblast activation and tissue fibrosis. *Nat Commun*. 2017;8(1):1130.
20. Yue H, Li W, Desnoyer R, Karnik SS. Role of nuclear unphosphorylated STAT3 in angiotensin II type 1 receptor-induced cardiac hypertrophy. *Cardiovasc Res*. 2010;85(1):90–99.
21. Parkinson NJ, et al. Mutant β-spectrin 4 causes auditory and motor neuropathies in quivering mice. *Nat Genet*. 2001;29(1):61–65.

22. Kanisicak O, et al. Genetic lineage tracing defines myofibroblast origin and function in the injured heart. *Nat Commun*. 2016;7:12260.
23. Li C, et al. Noncanonical STAT3 activation regulates excess TGF-β1 and collagen I expression in muscle of stricturing Crohn's disease. *J Immunol*. 2015;194(7):3422–3431.
24. Dobaczewski M, Chen W, Frangogiannis NG. Transforming growth factor (TGF)-β signaling in cardiac remodeling. *J Mol Cell Cardiol*. 2011;51(4):600–606.
25. Kaur H, et al. Targeted ablation of periostin-expressing activated fibroblasts prevents adverse cardiac remodeling in mice. *Circ Res*. 2016;118(12):1906–1917.
26. Meléndez GC, McLarty JL, Levick SP, Du Y, Janicki JS, Brower GL. Interleukin 6 mediates myocardial fibrosis, concentric hypertrophy, and diastolic dysfunction in rats. *Hypertension*. 2010;56(2):225–231.
27. Zhao L, et al. Deletion of interleukin-6 attenuates pressure overload-induced left ventricular hypertrophy and dysfunction. *Circ Res*. 2016;118(12):1918–1929.
28. Biernacka A, Dobaczewski M, Frangogiannis NG. TGF-β signaling in fibrosis. *Growth Factors*. 2011;29(5):196–202.
29. Khalil H, et al. Fibroblast-specific TGF-β-Smad2/3 signaling underlies cardiac fibrosis. *J Clin Invest*. 2017;127(10):3770–3783.
30. Tang Y, Katuri V, Dillner A, Mishra B, Deng CX, Mishra L. Disruption of transforming growth factor-β signaling in ELF β-spectrin-deficient mice. *Science*. 2003;299(5606):574–577.
31. Piersma B, Wouters OY, Bank RA. αII-spectrin and βII-spectrin do not affect TGFβ1-induced myofibroblast differentiation. *Cell Tissue Res*. 2018;374(1):165–175.
32. Christensen MD, Dun W, Boyden PA, Anderson ME, Mohler PJ, Hund TJ. Oxidized calmodulin kinase II regulates conduction following myocardial infarction: a computational analysis. *PLoS Comput Biol*. 2009;5(12):e1000583.
33. Hund TJ, et al. Role of activated CaMKII in abnormal calcium homeostasis and I(Na) remodeling after myocardial infarction: insights from mathematical modeling. *J Mol Cell Cardiol*. 2008;45(3):420–428.
34. Knierim E, et al. A recessive mutation in beta-IV-spectrin (SPTBN4) associates with congenital myopathy, neuropathy, and central deafness. *Hum Genet*. 2017;136(7):903–910.
35. Wang CC, et al. βIV spectrinopathies cause profound intellectual disability, congenital hypotonia, and motor axonal neuropathy. *Am J Hum Genet*. 2018;102(6):1158–1168.
36. Hund TJ, et al. β(IV)-Spectrin regulates TREK-1 membrane targeting in the heart. *Cardiovasc Res*. 2014;102(1):166–175.
37. Kakkar R, Lee RT. Intramyocardial fibroblast myocyte communication. *Circ Res*. 2010;106(1):47–57.
38. Molkentin JD, et al. Fibroblast-specific genetic manipulation of p38 mitogen-activated protein kinase in vivo reveals its central regulatory role in fibrosis. *Circulation*. 2017;136(6):549–561.
39. Howard T, et al. CaMKII-dependent late Na^+ current increases electrical dispersion and arrhythmia in ischemia-reperfusion. *Am J Physiol Heart Circ Physiol*. 2018;315(4):H794–H801.
40. George SA, et al. Extracellular sodium and potassium levels modulate cardiac conduction in mice heterozygous null for the Connexin43 gene. *Pflugers Arch*. 2015;467(11):2287–2297.
41. Gloschat C, et al. RHYTHM: an open source imaging toolkit for cardiac panoramic optical mapping. *Sci Rep*. 2018;8(1):2921.
42. Lafontant PJ, Burns AR, Donnachie E, Haudek SB, Smith CW, Entman ML. Oncostatin M differentially regulates CXC chemokines in mouse cardiac fibroblasts. *Am J Physiol Cell Physiol*. 2006;291(1):C18–C26.
43. Valiente-Alandi I, et al. Inhibiting fibronectin attenuates fibrosis and improves cardiac function in a model of heart failure. *Circulation*. 2018;138(12):1236–1252.
44. Cao W, Shi P, Ge JJ. miR-21 enhances cardiac fibrotic remodeling and fibroblast proliferation via CADM1/STAT3 pathway. *BMC Cardiovasc Disord*. 2017;17(1):88.
45. Stevenson MD, Sieminski AL, McLeod CM, Byfield FJ, Barocas VH, Gooch KJ. Pericellular conditions regulate extent of cell-mediated compaction of collagen gels. *Biophys J*. 2010;99(1):19–28.